Materials Science in Semiconductor Processing

Anatomy of Resistive Switching Behavior in Titanium Oxide Based RRAM Device

--Manuscript Draft--

Manuscript Number:	MSSP-D-21-01529R2
Article Type:	Research Paper
Section/Category:	Memory devices
Keywords:	Resistive Switching; Numerical Physics Model; oxygen vacancy; Metal oxide
Corresponding Author:	Yingtao Li Lanzhou University Lanzhou, CHINA
First Author:	Kuan Yang
Order of Authors:	Kuan Yang
	Liping Fu
	Junhao Chen
	Fangcong Wang
	Lixue Tian
	Xiaoqiang Song
	Zewei Wu
	Yingtao Li
Abstract:	Resistive random access memory (RRAM) devices based on binary transition metal oxides and the application for nonvolatile memory devices are becoming an area of extensive concern. The physical understanding of resistive switching is crucial for RRAM development. In this paper, both experiments and simulated dynamic formation and rupture processes of oxygen vacancy (V O) conductive filament (CF) channels in titanium oxide based RRAM devices are presented. Compared with the Al/TiO 2.1 /Al device with higher oxygen content, the Al/TiO 1.6 /Al device shows a lower forming voltage. However, little dependence on oxygen content in TiO x film is shown for other resistive switching parameters, including high resistance state resistance, low resistance state resistance, set voltage, and reset voltage. A kinetic Monte Carlo model is presented to relate the resistive switching behavior to the evolution CF channels in terms of V O morphology and I-V characteristics.
Response to Reviewers:	

Subject: Resubmission of the revised manuscript

Manuscript Number: MSSP-D-21-01529R1

Title: Anatomy of Resistive Switching Behavior in Titanium Oxide Based RRAM Device

Dear Editor,

Thanks very much for your Decision Letter about our manuscript (MSSP-D-21-01529R1), entitled "Anatomy of Resistive Switching Behavior in Titanium Oxide Based RRAM Device". We greatly appreciate the valuable and constructive comments from you and the reviewers. After several discussions, we have carefully addressed the critical comments pointed out by the reviewers in the response letter, and we have also explained the facts causing the difference and the relationship between resistance and CF thickness in the simulation.

The Reviewer #3 commented our work as "The manuscript has been revised according to previous reviewer's comments. It is believed that this paper is ready for publication." So, we believe that the importance of our paper makes it suitable for the publication of **Materials Science in Semiconductor Processing.**

Thanks very much for your attention to our paper. If you have any question about this paper, please don't hesitate to let me know

Yours Sincerely,

Yingtao Li

Highlights

Anatomy of Resistive Switching Behavior in Titanium Oxide Based RRAM Device

Kuan Yang,Liping Fu,Junhao Chen,Fangcong Wang,Lixue Tian,Xiaoqiang Song,Zewei Wu,Yingtao Li

- Effectively decrease forming voltage and operating energy of RRAM
- Explicitly analyse the switching behavior by stochastic numerical physics model
- Dynamically visualise evolution of conductive filaments to understand the mechanism

Dear Reviewers,

Thank you very much for your valuable and insightful comments for our manuscript (MSSP-D-21-01529R1), entitled "**Anatomy of Resistive Switching Behavior in Titanium Oxide Based RRAM Device**".

We feel that your comments and suggestions are fully inspirational and helpful. We have significantly revised the paper according to the constructive comments received from you. We hope that all the issues have been addressed appropriately. We would be grateful if you could take time to examine our detailed response regarding how we revise our manuscript on the following pages.

Your time and patience are highly appreciated! Please let me know should you require any additional information.

Yours Sincerely,

Yingtao Li, Ph. D

I. Comments from Reviewer #1

Comment 1: In this manuscript, authors claimed the simulation results can predict the oxygen vacancies after forming. However, there is lack of results like EDS mapping to confirm the simulation results.

Reply to Comment 1: Thank you very much for your comment. We highly appreciate the reviewer's suggestion to include advanced methods within the work on RRAM. We do believe such work is critical and meaningful, which could dramatically enhance the understanding of V_O profile after forming. While, the tough point is, the distribution of V_O and the morphology of CF are generally stochastic. It is challenging, considering our current conditions and facilities for experiments, to obtain the dynamics of V_O for the whole RS process by method like EDS mapping, and this is why we rely on simulation to discover the underlying mechanism. However, rest assured, we do firmly agree with your viewpoint of introducing these advanced techniques to further inspire and validate our investigation. We would painstakingly continue our research and expand our experimental methodology for purposes including validation.

On the other hand, the objective of our work is not limited to the prediction of V_O profile. Our pursuit is to elucidate the impact of different V_O concentration on the performance of the device, for which we introduce kMC simulation method to model the dynamics of V_O evolution. Moreover, the simulated results, for example, the *I-V* curve from simulation, coincides with the results from experiment. Hence, we hope the simulation part is still useful to support such objective in our manuscript.

Comment 2: In figure 3, the results show the same LRS after the set and the forming process. However, the simulation results show the LRS after the set process is thicker than the LRS after forming process. Could the authors explain the facts causing the difference and the relationship between resistance and CF thickness in the simulation?

Reply to Comment 2: Thanks very much for mentioning this point. In short, the resistance is dominantly determined by N, the number of V_O participating in tunneling when CF is formed.

Due to the changes in tunneling possibility, although N is highly correlated with number of V_O or CF thickness, the relation between N and CF thickness is slightly different from a proportional relation.

First of all, we revisit the Eqn(7) in the manuscript.

$$I = I_0 \exp(-\frac{a}{a_0})\sinh(\frac{V}{V_0}) + Nqv_d$$

Here, N is the number of traps participating in the tunneling process, where$N \propto n_D$.The first term $I_0 \exp(-\frac{a}{a_0})\sinh(\frac{V}{V_0})$ is the current flow generated by the V_O migration, and it is remarkably smaller than Nqv_d which measures the current flow comes from tunneling process when CF is formed. Since we are considering the relation between CF thickness and resistance (CF is formed), we left to consider the value of N. In other words, for larger N, we have larger I, and consequently, smaller resistance. Based on the relation $N \propto n_D$, generally, with more V_O, we have higher n_D, therefore smaller resistance.

However, note that, n_D is slightly different from being density of V_O. As from the manuscript, n_D comes from the density of V_O that participating in the tunneling process, hence, it is smaller than the density of V_O. We believe such difference is critical if we focus on the relation between resistance and CF thickness, hence we also modify our manuscript for clarification purposes.

"where n_D is the vertical density of oxygen vacancy participating in tunneling, which is computed by the configuration of V_O"

Apologize if this causes ambiguity.

Then we have enough armoury for the following explanation. The mechanism of $TiO_{1.6}$ and $TiO_{2.1}$ device is generally the same, hence, we would mainly elaborate on $TiO_{2.1}$ device.

For experiment part, Supplementary Fig. 1 shows the *I-V* curve where *I-V* curves from *I-V*

sweeping and forming are presented. In LRS, we could witness that the current of forming is slightly lower compared to that of *I-V* sweeping in the regime of 0.6V→0.0V. As we could judge from the simulation, this comes from the difference in CF thickness during these two phases.

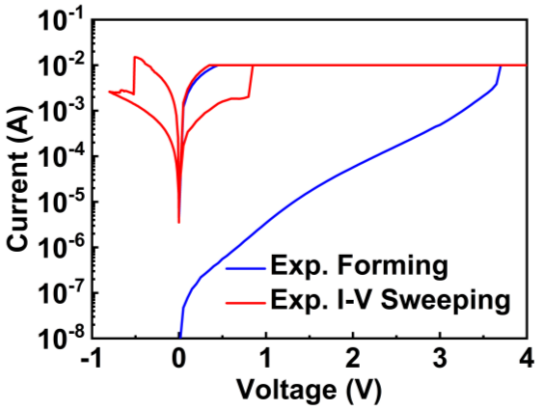

Supplementary Fig. 1. Experimental*I-V* curves during forming process and *I-V* sweepingprocess. The current of forming is slightly lower than that of *I-V* sweeping during 0.6V→0.0V.

Then, we proceed to the simulation part, whose *I-V* curves of sweeping and forming are presented in Supplementary Fig. 2.

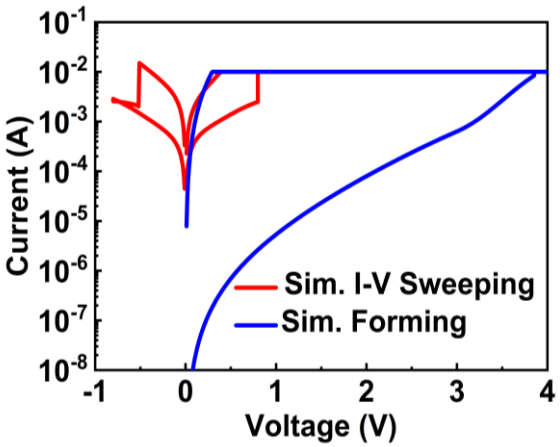

Supplementary Fig. 2. Simulated *I-V* curves during forming process and *I-V* sweeping process. The current of forming is slightly lower than that of *I-V* sweeping during 0.45V→0.0V.

The case of simulated curve generally follows the situation from experiment, while, the only deviation is, in the regime of 0.5V→0.45V, the current of *I-V* sweeping is slightly smaller than that

of forming. In other words, the *I-V* drops earlier. It is the distribution of V_O that increases the difficulty of tunneling, further reducing the n_D and I.

Before we explain details of this deviation, we would have to clarify the difference between the experiment and the simulation in obtaining the *I-V* characteristic curves, which is the root cause for this. For experiment, the *I-V* sweeping curve is obtained right after the forming process. However, the simulated sweeping curve is based on simulated V_O dynamics in Fig. 4, where the V_O profile during *I-V* sweeping is an average of 100 times of kMC simulation of the particle evolution.

It is already reported [1] and also witnessed in our simulation, the resistance of1st ON state is generally smaller compared to the following cycles.Based onour simulation, the reason is that, for the first few SET/RESET cycles, the CF would generally follow the morphology after forming process (like what we can see from Fig.4 (f) and (n)), which is ‘complete’ and ‘regular’. As the increase of *I-V* sweeping cycles, part of the CF, in particular the tip, would undergo abundant set and reset processes, therefore the tip of CF would be more and more ‘discrete’ and ‘random’, as what we can see from Fig. 4(h) and (p). Since the kMC would be iterated for 100 times, the simulated *I-V* sweeping is thus based on the discrete V_O profile, while, the experiment *I-V* curve comes from a more regular V_O distribution as it is captured right after the forming process.

The impact of the difference in V_O distribution contributes to the change in tunneling possibility. When the voltage is adequate, such discrete shape increases the difficulty of tunneling, since there are few paths but many electrons. In other words, although the CF is seemingly thicker, many of electrons are trapped in isolated V_O nano-islands due to the discrete shape of CF with insufficient conductive paths.However, when the voltage decreases, such phenomena would be

less important, since the electrons are fewer. In other words, even the CF is discrete, the conductive paths are still sufficient for the fewer electrons. Hence, when the voltage is smaller, we would witness the thicker CF generally brings lower resistance.

In order to support our viewpoint, we also supply an E-Map here. The E-Map illustrates the electrical field profile of our device. Generally, the larger electrical field would imply higher current density. We focus on the left region of the E-Map, which is the tip of CF. What we could see is that, the area of region with higher electrical field (brighter color means higher electrical field, here, it is the region with green color) in both two devices are generally the same, and the higher field region is disconnected in ON state. The reason is that, due to the discrete distribution of V_O that increases the difficulty of tunneling and conduction, and many electrons are trapped in V_O nano-islands. Therefore, the current could be slightly lower for *I-V* sweeping, although the CF is seemingly thicker compared to the forming state.

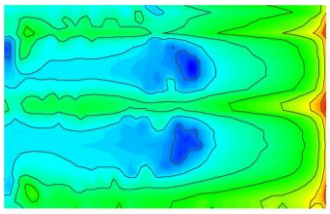

Supplementary Fig. 3: E-Map of $TiO_{2.1}$ device at 4V after forming process.

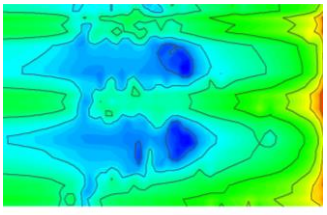

Supplementary Fig. 4: E-Map of $TiO_{2.1}$ device at ON state after SET process.

In conclusion, generally, the thicker the CF, the smaller the resistance. However, there could be small fluctuation, as illustrated in Fig. 2(a) in the manuscript, due to reasons including changes in distribution of V_O which affects the critical tunneling possibility.

[1]. Y. S. Chen et al., "Highly scalable hafnium oxide memory with improvements of resistive distribution and read disturb immunity," 2009 IEEE International Electron Devices Meeting (IEDM), 2009, pp. 1-4,

II. Comments from Reviewer #3

Comment 1: The manuscript has been revised according to previous reviewer's comments. It is believed that this paper is ready for publication.

Reply to Comment 1: Thank you very much for recommending our paper for publication.

Anatomy of Resistive Switching Behavior in Titanium Oxide Based RRAM Device

Kuan Yang[a,b,1], Liping Fu[a,1], Junhao Chen[c], Fangcong Wang[a,*], Lixue Tian[a], Xiaoqiang Song[a], Zewei Wu[a], Yingtao Li[a,*]

[a]*School of Physical Science and Technology, Lanzhou University, Lanzhou 730000, China*
[b]*Cuiying Honors College, Lanzhou University, Lanzhou 730000, China*
[c]*School of Mechanical Engineering, University of Leeds, Leeds LS2 9JT, United Kingdom*

Abstract

Resistive random access memory (RRAM) devices based on binary transition metal oxides and the application for nonvolatile memory devices are becoming an area of extensive concern. The physical understanding of resistive switching is crucial for RRAM development. In this paper, both experiments and simulated dynamic formation and rupture processes of oxygen vacancy (V_O) conductive filament (CF) channels in titanium oxide based RRAM devices are presented. Compared with the Al/$TiO_{2.1}$/Al device with higher oxygen content, the Al/$TiO_{1.6}$/Al device shows a lower forming voltage. However, little dependence on oxygen content in TiO_x film is shown for other resistive switching parameters, including high resistance state resistance, low resistance state resistance, set voltage, and reset voltage. A numerical physics model is presented to relate the resistive switching behavior with the evolution CF channels in terms of V_O morphology and $I-V$ characteristics.

Key words: Resistive Switching, Numerical Physics Model, Oxygen Vacancy, Metal Oxide

*Corresponding author: wangfc@lzu.edu.cn (F. Wang), li_yt06@lzu.edu.cn (Y. Li)
[1]K. Yang and L. Fu contribute equally to this work

1. Introduction

Resistive random access memory (RRAM) device based on the binary transition metal oxide is regarded as prospective choice for next-generation nonvolatile memory applications considering its simple structure, excellent scalability, fast speed, low power consumption, and high density [1–5]. Recently, abundant research has been done on titanium oxide film for RRAM applications due to its simple constitution and feasible compatibility with CMOS technology [6–9]. So far, various models, including power-induced mechanism [7], Schottky-emission-type conduction [8], and conductive filament (CF) channels [9], have been utilized to explain the resistive switching behaviors in TiO_x-based RRAM devices. Among existing models, the idea of the formation and disruption of CFs seems to be one of the most plausible [9, 10]. Moreover, the evolution and morphology of CFs are believed to affect the electrical performances of RRAM in terms of the forming and the subsequent resistive switching process [11, 12]. Nevertheless, the details of microscopic changes of CFs responsible for the resistive switching are still lacking, partly because the initial generation of CFs by electrical forming process is also poorly understood.

In this letter, in order to generalize the resistive switching behavior of TiO_x-based RRAM, we carry out an experimental analysis and also introduce a numerical physics model for insights into V_O CFs during the forming and the subsequent resistive switching process. The model can accurately capture the forming and $I-V$ characteristics of TiO_x-based RRAM devices with different oxygen content in TiO_x films. Such a comprehensive analysis of the V_O CFs formation and rupture would strongly aid the manufacturing of the TiO_x-based device for optimization purposes.

2. Experiments

The cross-point arrays $Al/TiO_x/Al$ memory devices with device areas of 20 μm $\times$20 μm were fabricated on SiO_2/Si substrates. 200 nm vertical lines of Al as bottom electrodes were first deposited by electron beam evaporation and

patterned through a lift-off process. Subsequently, $TiCl_4$ was used as the Ti precursor and H_2O was used as the oxygen precursor. An atomic layer deposition cycle with four steps was adopted for this experiment. The four steps were $TiCl_4$ reactant, N_2 purge, H_2O reactant, and N_2 purge, respectively. The pulse durations of the $TiCl_4$ and N_2 were 200 ms and 1500 ms, respectively. In order to investigate the effect of oxygen content on the resistive switching characteristics of titanium oxide films, two sets of TiO_x (30 nm) devices with different oxygen content were defined by the pulse durations of the H_2O with 250 ms and 450 ms, respectively. By using x-ray photoelectron spectroscopy (XPS) analyses, the oxygen to titanium ratio of the as prepared films for the two sets of TiO_x devices was about 1.6 and 2.1, respectively. Finally, 200 nm horizontal lines of Al as top electrodes were deposited by electron beam evaporation after the last lithography, and then another lift-off process was used to pattern the top electrodes. A Keithley 4200-SCS semiconductor characterization system was applied for measurement of all electrical characteristics. During the measurements, the top electrode was biased with the bottom electrode grounded.

3. Results and Discussion

Fig.1(a) shows the typical $I-V$ curves of the Al/$TiO_{2.1}$/Al and Al/$TiO_{1.6}$/Al devices. Both devices show high initial resistances, and to trigger the reversible resistive switching behaviors in both devices, an electroforming process through the utilization of a large positive voltage is essential. After the initial electroforming process, both devices can be switched from the low resistance state (LRS) to a high resistance state (HRS) (reset process) by applying a negative bias, and through a positive voltage to switch from the HRS to the LRS (set process) again, as shown in Fig.1(a). For each structure, a group of 20 fresh devices are selected randomly, and the statistics of the initial resistances (R_I) and forming voltages (V_F) are shown in Fig.1(b). For each structure, a group of 20 fresh devices are selected randomly, and the statistics of the initial resistances (R_I) and forming voltages (V_F) are shown in Fig.1(b),

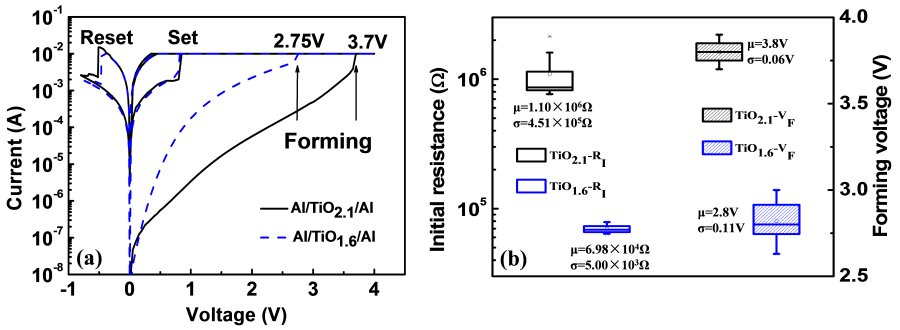

Figure 1: (a) Typical I-V curves of the Al/$TiO_{2.1}$/Al device and Al/$TiO_{1.6}$/Al device. (b) Statistical distributions of the initial resistances (R_I) and forming voltages (V_F) of both devices from 20 randomly chosen fresh devices.

in which $TiO_{2.1} - R_I$ and $TiO_{1.6} - R_I$ represent the initial resistances of the Al/$TiO_{2.1}$/Al and Al/$TiO_{1.6}$/Al device, and the $TiO_{2.1} - V_F$ and $TiO_{1.6} - V_F$ represent the forming voltages of the Al/$TiO_{2.1}$/Al and Al/$TiO_{1.6}$/Al device. It should be noted that the mean value (μ) of R_I for the Al/$TiO_{1.6}$/Al device is lower than that of the Al/$TiO_{2.1}$/Al devices, and the μ of V_F is reduced from 3.8 V to 2.8 V for the Al/$TiO_{1.6}$/Al device. The lower V_F is natural for the Al/$TiO_{1.6}$/Al device, as an active layer with lower O/Ti ratio shares relatively higher oxygen vacancy concentration [13], which contributes to the higher leakage current. It has been demonstrated that the forming voltage of RRAM device is partly controlled by the thickness of the oxide films. In other words, the forming voltage would drop as the film thickness decreases [14]. In our case, the large forming voltage is due to the fact that 30 nm TiO_x film was used, and it is conceivable that the forming voltage would decrease if a thinner film thickness is applied [14].

Fig.2(a) and Fig.2(b) show the device-to-device distributions of HRS resistance (R_H), LRS resistance (R_L), set voltage (V_S), and reset voltage (V_R) for both devices, all these statistical data are from the repeatability of the resistive switching loops. As shown in Fig.2, the μ of R_H, R_L, V_S and V_R for the two devices are almost the same, indicating that the resistive switching parameters,

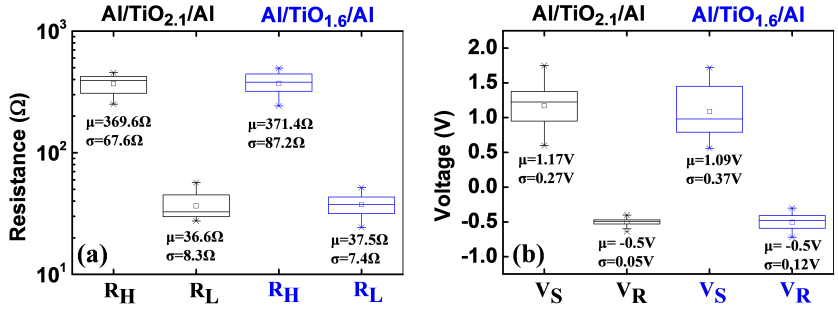

Figure 2: Statistical distributions of resistive switching parameters for the $Al/TiO_{2.1}/Al$ device and $Al/TiO_{1.6}/Al$ device. (a) HRS resistance (R_H) and LRS resistances (R_L), (b) set voltage (V_S) and reset voltage (V_R).

including R_H, R_L, V_S, and V_R, show little dependence on oxygen content in as-deposited TiO_x film.

To deeply investigate why these two devices behave so distinctively, a numerical physics model which takes factors temperature, electrical field, current density into consideration is presented based on Monte Carlo simulation to analyze the *I-V* characteristics and the related V_O CFs evolution during the forming and the subsequent resistive switching process. The simulation compromises two modules, including the calculation for generation and recombination of V_O, and the motion of O^{2-}, in addition, the configuration of electrical field and temperature which is essential for simulation is calculated as well. The results from the simulation show a straightforward dynamical process of formation and rupture of CFs.

At first, the filament region is split into grids of 30×60. To represent different types of TiO_x material, the computational domain is set to different initial state of V_O concentration and configuration. The generation and recombination of V_O are simulated according to the possibility in (1) and (2), respectively [15].

$$P_G = v\ \exp(-\frac{E_A\ -\ b\cdot F}{k_B\cdot T}) \tag{1}$$

$$P_R \;=\; v\,\exp(-\,\frac{E_{A,R}}{k_B\cdot T}) \tag{2}$$

where $v = 1.9\times10^{13}$ Hz is the effective vibration frequency of the O-Ti bonds[16], $E_A = 2.02eV$ [17] is the zero-field effective activation energy required to break the Ti-O bond, F is the local electrical field, b is the bond polarization factor, taken as $180e\mathring{A}$ in our simulation, which is in good agreement with reported experimental result [15]. $E_{A,R} = 0.2eV$ is the activation energy, and k_B, T are Bolzamn constant and local temperature, respectively [15].

The motion of oxygen ion at grid i is modelled based on its rate R_D[15], given by:

$$R_D = v\,\exp\left(-\frac{E_{A,D} - k_D\cdot F_D}{k_B\cdot T}\right) \tag{3}$$

$E_{A,D}$ is equal to $0.7eV$ for oxygen ions, and $k_D = qd_0\lambda$ is a factor accounting for the field-induced energy barrier reduction [18], where $d_0 = 5\times10^{-10}$m is the mesh size in simulation, and $\lambda\cdot d_0 = |i-j|\cdot d_0$ denotes the distance to the available grid j from grid i. F_D is the electrical field along the diffusion direction [15].

The local temperature T is solved by the Fourier equation[19], namely

$$\nabla k_{th}\nabla T = \sigma\,|\nabla V|^2 \tag{4}$$

where k_{th}, σ are thermal conductivity and electrical conductivity, respectively, which are variables to temperature or V_O concentration. The electrical conductivity σ is given by[20]

$$\sigma = \sigma_0 \exp\left(-\frac{E_{AC}}{k_B T}\right) \tag{5}$$

where σ_0 is the pre-exponential factor, E_{AC} is the activation energy for electrical conduction [21].

The electrical field F and F_D are solved by Poisson Equation, namely

$$\nabla^2\phi = -\frac{\rho}{\epsilon_0} \tag{6}$$

with the boundary condition as $\phi = 0$ and $\phi = V_d$, where V_d is the applied bias, ρ is the distribution of charges, and ϵ_0 is the permittivity of the free space.

Moreover, we calculate the current by combining the ionic conduction of the V_O, and the conduction through electrons. Hence, the current can be calculated by the following equation [21],

$$I = I_0 \exp\left(-\frac{a}{a_0}\right) \sinh\left(\frac{V}{V_0}\right) + Nqv_d \tag{7}$$

where $I_0 \approx 0.1nA, a \approx 1nm, a_0 \approx 0.05nm, V_0 \approx 0.4V$[16] are parameters of the hopping conduction of V_O at the low bias region. N is the number of traps participating in the tunneling process given by

$$N = n_D \cdot n_0 \tag{8}$$

where n_D is the vertical oxygen vacancy participating in tunnelling, which is computed by the configuration of V_O, and $n_0 \sim 10^{16}$ is the parameter obtained by curve fitting at LRS region since the n_D we obtained is in 2D cross section, and we have to amplify it to satisfy the conduction in 3D scale, and v_d is the transition rate, given by [21, 22]

$$v_d = a_d \cdot v_0 \cdot \exp\left(-\frac{E_a}{k_B T}\right) \cdot \sinh\left(\frac{2qFa_d}{k_B T}\right) \tag{9}$$

where F is the local electrical field solved by (6), $a_d = 0.1nm$ is the effective hopping distance, v_0 is the attempt-to-escape frequency of 10^{13} Hz [21, 22].

Finally, we combine all the equations with the framework of the numerical model. After providing the model with the initial condition, we could subsequently calculate the evolution of V_O, and update the temperature and electric field. We would keep iterating the computation till the system approaches the convergence under the given bias. The system would prompt to the next step of bias once it converges.

Fig.3(a) and Fig.3(b) show the simulated and the experimental curves of forming process and subsequent resistive switching for the Al/$TiO_{2.1}$/Al device and Al/$TiO_{1.6}$/Al device, respectively. It is noted that the simulated results agree well with experimental data for both devices. The forming process and the consequent resistive switching characteristics are well captured by the analytical model.

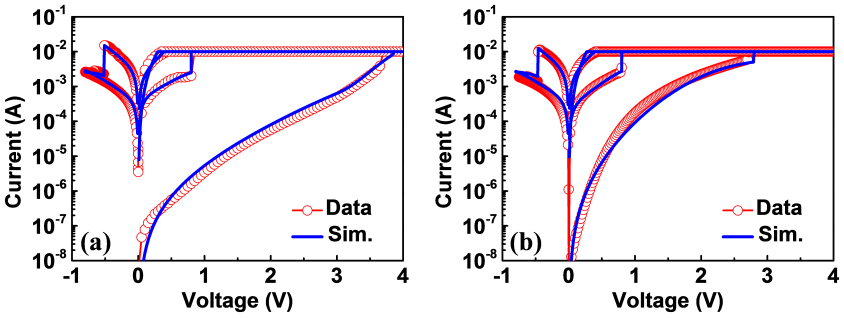

Figure 3: Comparison between experimental and simulated I-V characteristics of (a) Al/$TiO_{2.1}$/Al device and (b) Al/$TiO_{1.6}$/Al device.

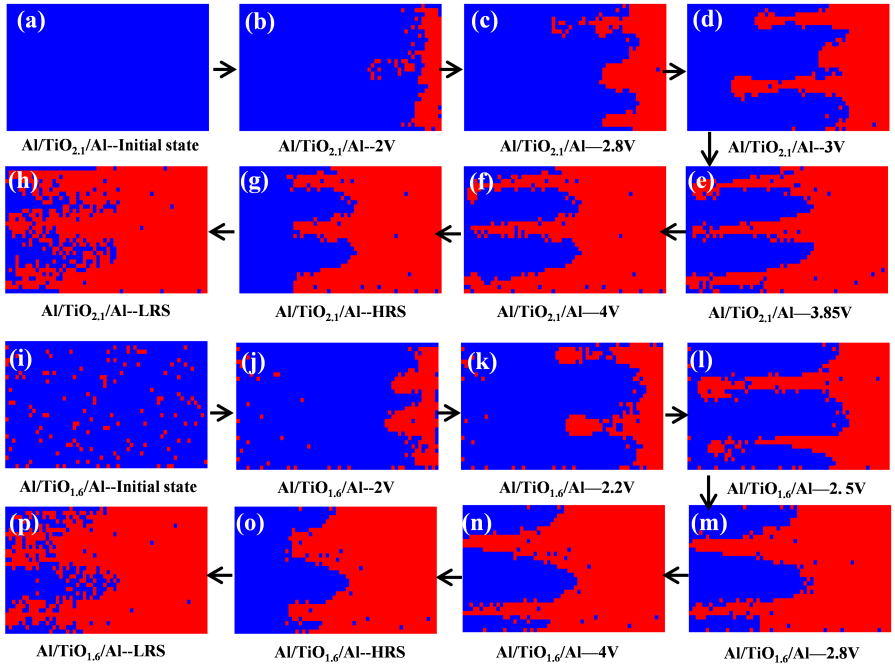

Figure 4: Simulated dynamic structure evolution of V_O CFs in both Al/$TiO_{2.1}$/Al device (a-h) and Al/$TiO_{1.6}$/Al device (i-p).

Dynamics of V_O migration effect on CFs growth in TiO_x films is analyzed afterwards. To ensure the representativeness of the results, we iterate the simulation for 100 times. Fig. 4 shows the simulated dynamic evolution of V_O

CFs during the forming and the subsequent resistive switching process for both $Al/TiO_{2.1}/Al$ device (images a-h) and $Al/TiO_{1.6}/Al$ device (images i-p). For $Al/TiO_{2.1}/Al$ device, the CF grows from the bottom of the device, and it continues to grow as the bias increases. The tip of the CF extends gradually, and it finally reaches the top side of the device at 3.85V. Then, the CF grows thicker when the bias keeps increasing. When resetting the device, the CF breaks at the tip near the top electrode and it resumes when a positive bias is applied in SET process. The case of $Al/TiO_{1.6}/Al$ is similar, however, the CF grows faster and is thicker. To be specific, for the $Al/TiO_{2.1}/Al$ device, V_O CFs bridge the top electrode and bottom electrode when the voltage reaches 3.85 V. However, for the $Al/TiO_{1.6}/Al$ device, V_O CF channels form once the voltage increases to 2.8 V. This happens because more V_Os exist in the $TiO_{1.6}$ film than the $TiO_{2.1}$ film. Therefore, compared with the $Al/TiO_{2.1}/Al$ device, a lower voltage is enough to form the V_O CF channels in the $Al/TiO_{1.6}/Al$ device. Furthermore, when the voltage increases to 4 V, the morphology of CF channels in the $Al/TiO_{1.6}/Al$ device (image n) is quite similar to that in the $Al/TiO_{2.1}/Al$ device (image f). Evidently, in the case of the subsequent resistive switching process, the morphology of CF channels of both HRS (image g versus image o) and LRS (image h versus image p) in the two devices is similar. Thus, the R_H and R_L of the two devices are almost the same, as shown in Fig.2(a).

4. Conclusion

In summary, an experimental analysis was performed to investigate the effect of oxygen content in titanium oxide films on the performance of $Al/TiO_x/Al$ RRAM devices. In addition, a numerical physics model was presented to describe the detailed evolution of the formation and rupture of V_O CFs during the forming and the subsequent resistive switching process. The simulated *I-V* characteristics are in good agreement with the experimental data, which enhances the understanding towards the underlying mechanism of resistive switching and can further optimize the performance of a metal oxide-based RRAM device.

Acknowledgements

This work was supported by the National Natural Science Foundation of China (Grant No. 61774079), the Science and Technology Plan of Gansu Province (No. 20JR5RA307), the Key Talent Project of Organization Department in Gansu Province, the Hui-Chun Chin and Tsung-Dao Lee Chinese Undergraduate Research Endowment (LZU - JZH2239), and the Cuiying Foundation.

References

[1] R. Waser, M. Aono, Nature Materials 6 (2007) 833.

[2] Y. C. Yang, F. Pan, Q. Liu, M. Liu, F. Zeng, Nano Letters 9 (4) (2009) 1636.

[3] Y. Li, S. Long, M. Zhang, Q. Liu, L. Shao, S. Zhang, Y. Wang, Q. Zuo, S. Liu, M. Liu, IEEE Electron Device Letters 31 (2) (2010) 117.

[4] C. Li, D. Belkin, Y. Li, P. Yan, M. Hu, N. Ge, H. Jiang, E. Montgomery, P. Lin, Z. Wang, W. Song, J. P. Strachan, M. Barnell, Q. Wu, R. S. Williams, J. J. Yang, Q. Xia, Nature Communications 9 (1) (2018) 2385.

[5] X. Zhao, J. Ma, X. Xiao, Q. Liu, L. Shao, D. Chen, S. Liu, J. Niu, X. Zhang, Y. Wang, R. Cao, W. Wang, Z. Di, H. Lv, S. Long, M. Liu, Advanced Materials 30 (14) (2018) 1705193.

[6] H. Shima, F. Takano, H. Muramatsu, H. Akinaga, I. H. Inoue, H. Takagi, Applied Physics Letters 92 (4) (2008) 043510.

[7] C. Rohde, B. J. Choi, D. S. Jeong, S. Choi, J.-S. Zhao, C. S. Hwang, Applied Physics Letters 86 (26) (2005) 262907.

[8] W. Wang, S. Fujita, S. S. Wong, IEEE Electron Device Letters 30 (7) (2009) 763.

[9] J. J. Yang, F. Miao, M. D. Pickett, D. A. A. Ohlberg, D. R. Stewart, C. N. Lau, R. S. Williams, Nanotechnology 20 (21) (2009) 215201.

[10] J. J. Yang, M. D. Pickett, X. Li, D. A. A. Ohlberg, D. R. Stewart, R. S. Williams, Nature Nanotechnology 3 (7) (2008) 429.

[11] Y. Lu, B. Gao, Y. Fu, B. Chen, L. Liu, X. Liu, J. Kang, IEEE Electron Device Letters 33 (3) (2012) 306.

[12] B. Gao, S. Yu, N. Xu, L. F. Liu, B. Sun, X. Y. Liu, R. Q. Han, J. F. Kang, B. Yu, Y. Y. Wang, 2008 IEEE International Electron Devices Meeting (2008) 1.

[13] G. H. Baek, A. R. Lee, T. Y. Kim, H. S. Im, J. P. Hong, Applied Physics Letters 109 (14) (2016) 143502.

[14] C. C. Hsieh, A. Roy, A. Rai, Y. F. Chang, S. K. Banerjee, Applied Physics Letters 106 (17) (2015) 173108.

[15] A. Padovani, L. Larcher, O. Pirrotta, L. Vandelli, G. Bersuker, IEEE Transactions on Electron Devices 62 (6) (2015) 1998.

[16] K. Jalili, S. Aghabeygi, B. Mirza, Journal of Applied Chemical Research 10 (4) (2016) 123.

[17] E. N. Plotnikov, V. L. Stolyarova, Physics and Chemistry of Glasses 46 (2) (2005) 187.

[18] Wen Wu, Xiaodong Duan, J. S. Yuan, IEEE Transactions on Device and Materials Reliability 3 (2) (2003) 26.

[19] S. Srivastava, P. Dey, S. Asapu, T. Maiti, Nanotechnology 29 (50) (2018) 505702.

[20] D. Mardare, C. Baban, R. Gavrila, M. Modreanu, G. Rusu, Surface Science 507-510 (2002) 468.

[21] P. Bousoulas, I. Giannopoulos, P. Asenov, I. Karageorgiou, D. Tsoukalas, Journal of Applied Physics 121 (9) (2017) 094501.

[22] S. Yu, H. P. Wong, IEEE Electron Device Letters 31 (12) (2010) 1455.

Highlights

Anatomy of Resistive Switching Behavior in Titanium Oxide Based RRAM Device

Kuan Yang,Liping Fu,Junhao Chen,Fangcong Wang,Lixue Tian,Xiaoqiang Song,Zewei Wu,Yingtao Li

- Effectively decrease forming voltage and operating energy of RRAM
- Explicitly analyse the switching behavior by stochastic numerical physics model
- Dynamically visualise evolution of conductive filaments to understand the mechanism

Anatomy of Resistive Switching Behavior in Titanium Oxide Based RRAM Device

Kuan Yang[a,b,1], Liping Fu[a,1], Junhao Chen[c], Fangcong Wang[a], Lixue Tian[a], Xiaoqiang Song[a], Zewei Wu[a] and Yingtao Li[a]

[a]School of Physical Science and Technology, Lanzhou University, Lanzhou, 730000, China
[b]Cuiying Honors College, Lanzhou University, Lanzhou, 730000, China
[c]School of Mechanical Engineering, University of Leeds, Leeds, LS2 9JT, United Kingdom

ARTICLE INFO

Keywords:
Resistive Switching
Numerical Physics Model
Oxygen Vacancy
Metal Oxide

ABSTRACT

Resistive random access memory (RRAM) devices based on binary transition metal oxides and the application for nonvolatile memory devices are becoming an area of extensive concern. The physical understanding of resistive switching is crucial for RRAM development. In this paper, both experiments and simulated dynamic formation and rupture processes of oxygen vacancy (V_O) conductive filament (CF) channels in titanium oxide based RRAM devices are presented. Compared with the Al/$TiO_{2.1}$/Al device with higher oxygen content, the Al/$TiO_{1.6}$/Al device shows a lower forming voltage. However, little dependence on oxygen content in TiO_x film is shown for other resistive switching parameters, including high resistance state resistance, low resistance state resistance, set voltage, and reset voltage. A numerical physics model is presented to relate the resistive switching behavior with the evolution CF channels in terms of V_O morphology and $I-V$ characteristics.

1. Introduction

Resistive random access memory (RRAM) device based on the binary transition metal oxide is regarded as prospective choice for next-generation nonvolatile memory applications considering its simple structure, excellent scalability, fast speed, low power consumption, and high density [1–5]. Recently, abundant research has been done on titanium oxide film for RRAM applications due to its simple constitution and feasible compatibility with CMOS technology [6–9]. So far, various models, including power-induced mechanism [7], Schottky-emission-type conduction [8], and conductive filament (CF) channels [9], have been utilized to explain the resistive switching behaviors in TiO_x-based RRAM devices. Among existing models, the idea of the formation and disruption of CFs seems to be one of the most plausible [9, 10]. Moreover, the evolution and morphology of CFs are believed to affect the electrical performances of RRAM in terms of the forming and the subsequent resistive switching process [11, 12]. Nevertheless, the details of microscopic changes of CFs responsible for the resistive switching are still lacking, partly because the initial generation of CFs by electrical forming process is also poorly understood.

In this letter, in order to generalize the resistive switching behavior of TiO_x-based RRAM, we carry out an experimental analysis and also introduce a numerical physics model for insights into V_O CFs during the forming and the subsequent resistive switching process. The model can accurately capture the forming and $I-V$ characteristics of TiO_x-based RRAM devices with different oxygen content in TiO_x films. Such a comprehensive analysis of the V_O CFs formation and rupture would strongly aid the manufacturing of the TiO_x-based device for optimization purposes.

2. Experiments

The cross-point arrays Al/TiO_x/Al memory devices with device areas of 20 μm ×20 μm were fabricated on SiO_2/Si substrates. 200 nm vertical lines of Al as bottom electrodes were first deposited by electron beam evaporation and patterned through a lift-off process. Subsequently, $TiCl_4$ was used as the Ti precursor and H_2O was used as the oxygen precursor. An atomic layer deposition cycle with four steps was adopted for this experiment. The four steps were

*Corresponding author
wangfc@lzu.edu.cn (F. Wang); li_yt06@lzu.edu.cn (Y. Li)
ORCID(s):
[1]K. Yang and L. Fu contribute equally to this work

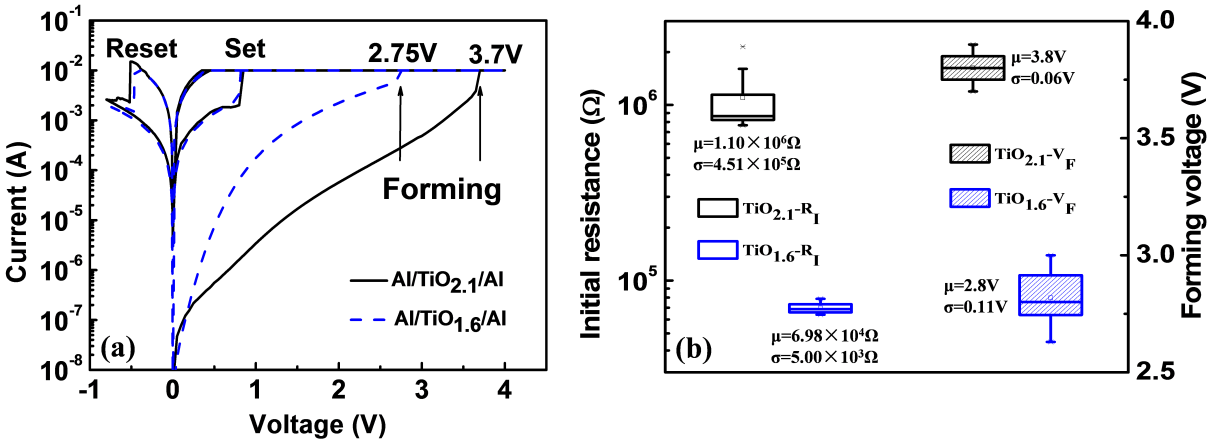

Figure 1: (a) Typical *I-V* curves of the Al/$TiO_{2.1}$/Al device and Al/$TiO_{1.6}$/Al device. (b) Statistical distributions of the initial resistances (R_I) and forming voltages (V_F) of both devices from 20 randomly chosen fresh devices.

$TiCl_4$ reactant, N_2 purge, H_2O reactant, and N_2 purge, respectively. The pulse durations of the $TiCl_4$ and N_2 were 200 ms and 1500 ms, respectively. In order to investigate the effect of oxygen content on the resistive switching characteristics of titanium oxide films, two sets of TiO_x (30 nm) devices with different oxygen content were defined by the pulse durations of the H_2O with 250 ms and 450 ms, respectively. By using x-ray photoelectron spectroscopy (XPS) analyses, the oxygen to titanium ratio of the as prepared films for the two sets of TiO_x devices was about 1.6 and 2.1, respectively. Finally, 200 nm horizontal lines of Al as top electrodes were deposited by electron beam evaporation after the last lithography, and then another lift-off process was used to pattern the top electrodes. A Keithley 4200-SCS semiconductor characterization system was applied for measurement of all electrical characteristics. During the measurements, the top electrode was biased with the bottom electrode grounded.

3. Results and Discussion

Fig.1(a) shows the typical $I-V$ curves of the Al/$TiO_{2.1}$/Al and Al/$TiO_{1.6}$/Al devices. Both devices show high initial resistances, and to trigger the reversible resistive switching behaviors in both devices, an electroforming process through the utilization of a large positive voltage is essential. After the initial electroforming process, both devices can be switched from the low resistance state (LRS) to a high resistance state (HRS) (reset process) by applying a negative bias, and through a positive voltage to switch from the HRS to the LRS (set process) again, as shown in Fig.1(a). For each structure, a group of 20 fresh devices are selected randomly, and the statistics of the initial resistances (R_I) and forming voltages (V_F) are shown in Fig.1(b). For each structure, a group of 20 fresh devices are selected randomly, and the statistics of the initial resistances (R_I) and forming voltages (V_F) are shown in Fig.1(b), in which $TiO_{2.1}-R_I$ and $TiO_{1.6}-R_I$ represent the initial resistances of the Al/$TiO_{2.1}$/Al and Al/$TiO_{1.6}$/Al device, and the $TiO_{2.1}-V_F$ and $TiO_{1.6}-V_F$ represent the forming voltages of the Al/$TiO_{2.1}$/Al and Al/$TiO_{1.6}$/Al device. It should be noted that the mean value (μ) of R_I for the Al/$TiO_{1.6}$/Al device is lower than that of the Al/$TiO_{2.1}$/Al devices, and the μ of V_F is reduced from 3.8 V to 2.8 V for the Al/$TiO_{1.6}$/Al device. The lower V_F is natural for the Al/$TiO_{1.6}$/Al device, as an active layer with lower O/Ti ratio shares relatively higher oxygen vacancy concentration [13], which contributes to the higher leakage current. It has been demonstrated that the forming voltage of RRAM device is partly controlled by the thickness of the oxide films. In other words, the forming voltage would drop as the film thickness decreases [14]. In our case, the large forming voltage is due to the fact that 30 nm TiO_x film was used, and it is conceivable that the forming voltage would decrease if a thinner film thickness is applied [14].

Fig.2(a) and Fig.2(b) show the device-to-device distributions of HRS resistance (R_H), LRS resistance (R_L), set voltage (V_S), and reset voltage (V_R) for both devices, all these statistical data are from the repeatability of the resistive switching loops. As shown in Fig.2, the μ of R_H, R_L, V_S and V_R for the two devices are almost the same, indicating

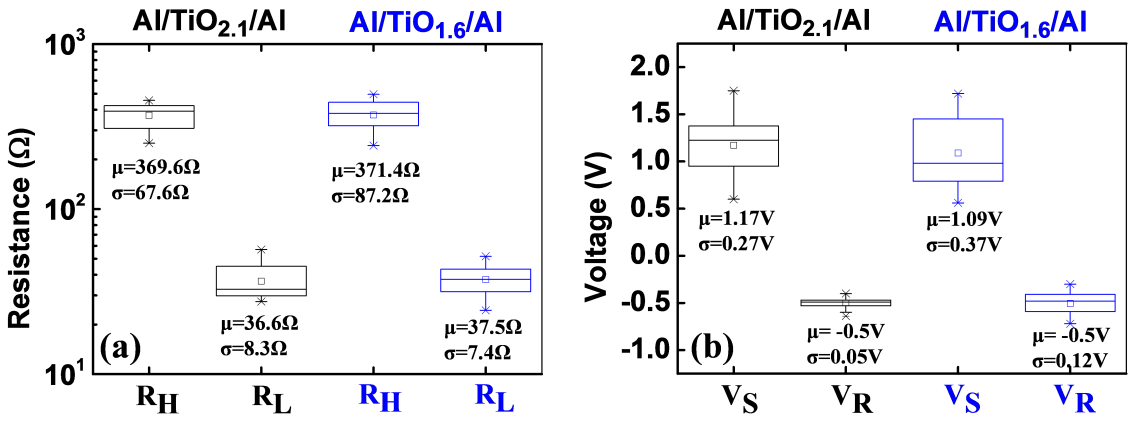

Figure 2: Statistical distributions of resistive switching parameters for the $Al/TiO_{2.1}/Al$ device and $Al/TiO_{1.6}/Al$ device. (a) HRS resistance (R_H) and LRS resistances (R_L), (b) set voltage (V_S) and reset voltage (V_R).

that the resistive switching parameters, including R_H, R_L, V_S, and V_R, show little dependence on oxygen content in as-deposited TiO_x film.

To deeply investigate why these two devices behave so distinctively, a numerical physics model which takes factors temperature, electrical field, current density into consideration is presented based on Monte Carlo simulation to analyze the *I-V* characteristics and the related V_O CFs evolution during the forming and the subsequent resistive switching process. The simulation compromises two modules, including the calculation for generation and recombination of V_O, and the motion of O^{2-}, in addition, the configuration of electrical field and temperature which is essential for simulation is calculated as well. The results from the simulation show a straightforward dynamical process of formation and rupture of CFs.

At first, the filament region is split into grids of 30×60. To represent different types of TiO_x material, the computational domain is set to different initial state of V_O concentration and configuration. The generation and recombination of V_O are simulated according to the possibility in (1) and (2), respectively [15].

$$P_G = \upsilon \exp(-\frac{E_A - b \cdot F}{k_B \cdot T}) \tag{1}$$

$$P_R = \upsilon \exp(-\frac{E_{A,R}}{k_B \cdot T}) \tag{2}$$

where $\upsilon = 1.9 \times 10^{13}$ Hz is the effective vibration frequency of the O-Ti bonds[16], $E_A = 2.02eV$ [17] is the zero-field effective activation energy required to break the Ti-O bond, F is the local electrical field, b is the bond polarization factor, taken as $180e\mathring{A}$ in our simulation, which is in good agreement with reported experimental result [15]. $E_{A,R} = 0.2eV$ is the activation energy, and k_B, T are Bolzamn constant and local temperature, respectively [15].

The motion of oxygen ion at grid i is modelled based on its rate R_D[15], given by:

$$R_D = \upsilon \exp\left(-\frac{E_{A,D} - k_D \cdot F_D}{k_B \cdot T}\right) \tag{3}$$

$E_{A,D}$ is equal to $0.7eV$ for oxygen ions, and $k_D = qd_0\lambda$ is a factor accounting for the field-induced energy barrier reduction [18], where $d_0 = 5 \times 10^{-10}$m is the mesh size in simulation, and $\lambda \cdot d_0 = |i - j| \cdot d_0$ denotes the distance to the available grid j from grid i. F_D is the electrical field along the diffusion direction [15].

The local temperature T is solved by the Fourier equation[19], namely

$$\nabla k_{th} \nabla T = \sigma |\nabla V|^2 \tag{4}$$

where k_{th}, σ are thermal conductivity and electrical conductivity, respectively, which are variables to temperature or V_O concentration. The electrical conductivity σ is given by[20]

$$\sigma = \sigma_0 \exp\left(-\frac{E_{AC}}{k_B T}\right) \tag{5}$$

where σ_0 is the pre-exponential factor, E_{AC} is the activation energy for electrical conduction [21].

The electrical field F and F_D are solved by Poisson Equation, namely

$$\nabla^2 \phi = -\frac{\rho}{\epsilon_0} \tag{6}$$

with the boundary condition as $\phi = 0$ and $\phi = V_d$, where V_d is the applied bias, ρ is the distribution of charges, and ϵ_0 is the permittivity of the free space.

Moreover, we calculate the current by combining the ionic conduction of the V_O, and the conduction through electrons. Hence, the current can be calculated by the following equation [21],

$$I = I_0 \exp\left(-\frac{a}{a_0}\right) \sinh\left(\frac{V}{V_0}\right) + N q v_d \tag{7}$$

where $I_0 \approx 0.1nA, a \approx 1nm, a_0 \approx 0.05nm, V_0 \approx 0.4V$ [16] are parameters of the hopping conduction of V_O at the low bias region. N is the number of traps participating in the tunneling process given by

$$N = n_D \cdot n_0 \tag{8}$$

where n_D is the vertical oxygen vacancy participating in tunnelling, which is computed by the configuration of V_O, and $n_0 \sim 10^{16}$ is the parameter obtained by curve fitting at LRS region since the n_D we obtained is in 2D cross section, and we have to amplify it to satisfy the conduction in 3D scale, and v_d is the transition rate, given by [21, 22]

$$v_d = a_d \cdot v_0 \cdot \exp\left(-\frac{E_a}{k_B T}\right) \cdot \sinh\left(\frac{2qFa_d}{k_B T}\right) \tag{9}$$

where F is the local electrical field solved by (6), $a_d = 0.1nm$ is the effective hopping distance, v_0 is the attempt-to-escape frequency of 10^{13} Hz [21, 22].

Finally, we combine all the equations with the framework of the numerical model. After providing the model with the initial condition, we could subsequently calculate the evolution of V_O, and update the temperature and electric field. We would keep iterating the computation till the system approaches the convergence under the given bias. The system would prompt to the next step of bias once it converges.

Fig.3(a) and Fig.3(b) show the simulated and the experimental curves of forming process and subsequent resistive switching for the Al/$TiO_{2.1}$/Al device and Al/$TiO_{1.6}$/Al device, respectively. It is noted that the simulated results agree well with experimental data for both devices. The forming process and the consequent resistive switching characteristics are well captured by the analytical model.

Dynamics of V_O migration effect on CFs growth in TiO_x films is analyzed afterwards. To ensure the representativeness of the results, we iterate the simulation for 100 times. Fig. 4 shows the simulated dynamic evolution of V_O CFs during the forming and the subsequent resistive switching process for both Al/$TiO_{2.1}$/Al device (images a-h) and Al/$TiO_{1.6}$/Al device (images i-p). For Al/$TiO_{2.1}$/Al device, the CF grows from the bottom of the device, and it continues to grow as the bias increases. The tip of the CF extends gradually, and it finally reaches the top side of the device at 3.85V. Then, the CF grows thicker when the bias keeps increasing. When resetting the device, the CF breaks at the tip near the top electrode and it resumes when a positive bias is applied in SET process. The case of Al/$TiO_{1.6}$/Al is similar, however, the CF grows faster and is thicker. To be specific, for the Al/$TiO_{2.1}$/Al device, V_O CFs bridge the top electrode and bottom electrode when the voltage reaches 3.85 V. However, for the Al/$TiO_{1.6}$/Al device, V_O CF channels form once the voltage increases to 2.8 V. This happens because more V_Os exist in the $TiO_{1.6}$ film than the $TiO_{2.1}$ film. Therefore, compared with the Al/$TiO_{2.1}$/Al device, a lower voltage is enough to form the V_O CF channels in the Al/$TiO_{1.6}$/Al device. Furthermore, when the voltage increases to 4 V, the morphology of CF channels in the Al/$TiO_{1.6}$/Al device (image n) is quite similar to that in the Al/$TiO_{2.1}$/Al device (image f). Evidently, in the case of the subsequent resistive switching process, the morphology of CF channels of both HRS (image g versus image o) and LRS (image h versus image p) in the two devices is similar. Thus, the R_H and R_L of the two devices are almost the same, as shown in Fig.2(a).

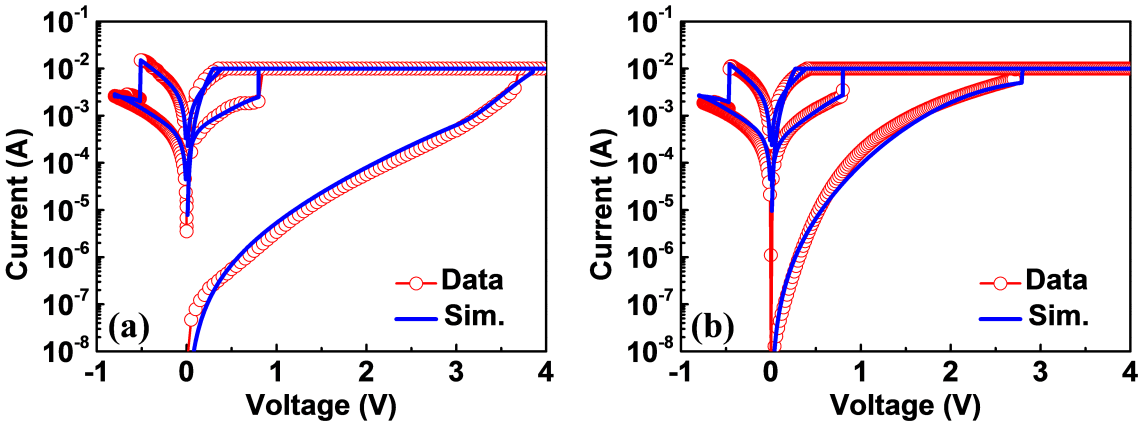

Figure 3: Comparison between experimental and simulated *I-V* characteristics of (a) Al/$TiO_{2.1}$/Al device and (b) Al/$TiO_{1.6}$/Al device.

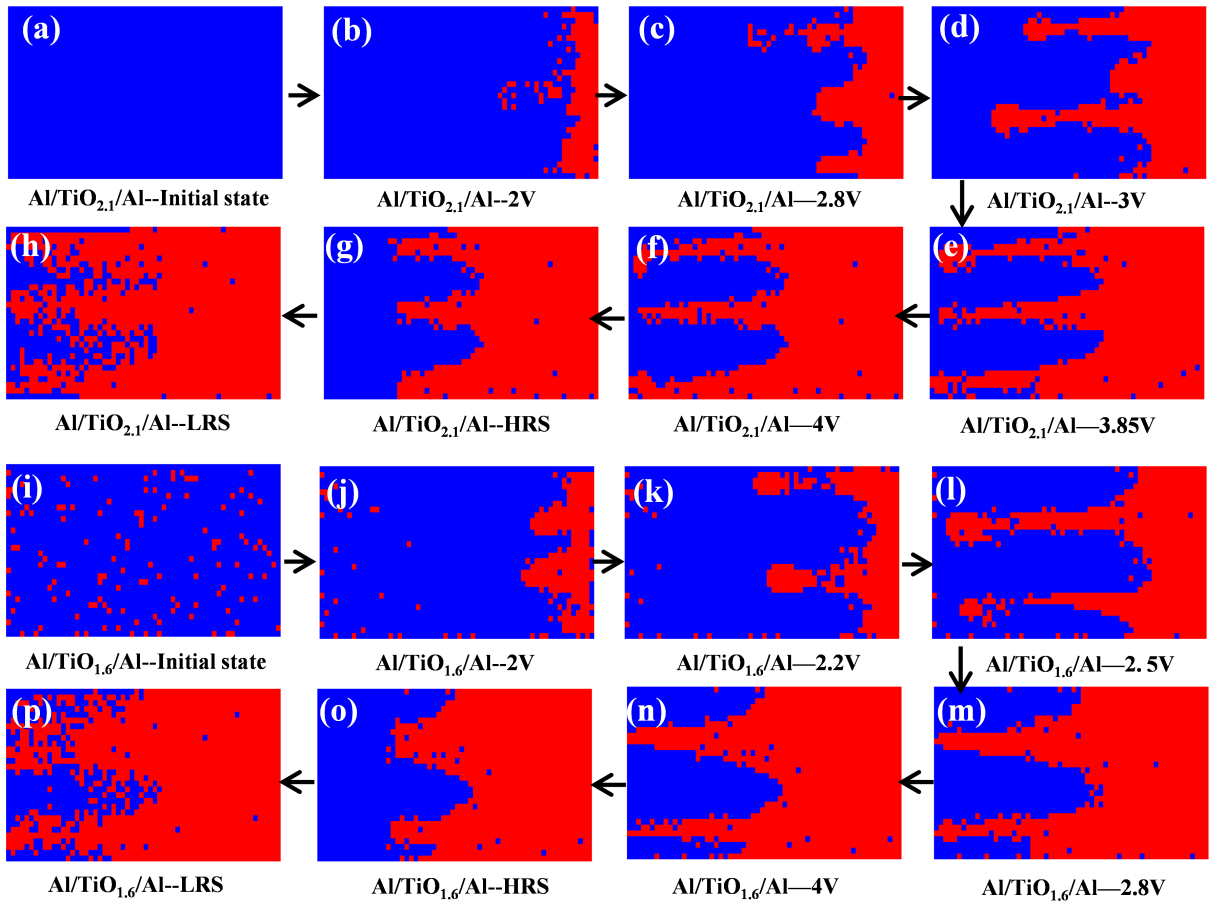

Figure 4: Simulated dynamic structure evolution of V_O CFs in both Al/$TiO_{2.1}$/Al device (a-h) and Al/$TiO_{1.6}$/Al device (i-p).

4. Conclusion

In summary, an experimental analysis was performed to investigate the effect of oxygen content in titanium oxide films on the performance of Al/TiO_x/Al RRAM devices. In addition, a numerical physics model was presented to describe the detailed evolution of the formation and rupture of V_O CFs during the forming and the subsequent resistive switching process. The simulated *I-V* characteristics are in good agreement with the experimental data, which enhances the understanding towards the underlying mechanism of resistive switching and can further optimize the performance of a metal oxide-based RRAM device.

Acknowledgements

This work was supported by the National Natural Science Foundation of China (Grant No. 61774079), the Science and Technology Plan of Gansu Province (No. 20JR5RA307), the Key Talent Project of Organization Department in Gansu Province, the Hui-Chun Chin and Tsung-Dao Lee Chinese Undergraduate Research Endowment (LZU - JZH2239), and the Cuiying Foundation.

References

[1] Waser R and Aono M 2007 *Nature Materials* **6**(11) 833
[2] Yang Y C, Pan F, Liu Q, Liu M and Zeng F 2009 *Nano Letters* **9** 1636
[3] Li Y, Long S, Zhang M, Liu Q, Shao L, Zhang S, Wang Y, Zuo Q, Liu S and Liu M 2010 *IEEE Electron Device Letters* **31** 117 ISSN 1558-0563
[4] Li C, Belkin D, Li Y, Yan P, Hu M, Ge N, Jiang H, Montgomery E, Lin P, Wang Z, Song W, Strachan J P, Barnell M, Wu Q, Williams R S, Yang J J and Xia Q 2018 *Nature Communications* **9** 2385 ISSN 2041-1723
[5] Zhao X, Ma J, Xiao X, Liu Q, Shao L, Chen D, Liu S, Niu J, Zhang X, Wang Y, Cao R, Wang W, Di Z, Lv H, Long S and Liu M 2018 *Advanced Materials* **30** 1705193
[6] Shima H, Takano F, Muramatsu H, Akinaga H, Inoue I H and Takagi H 2008 *Applied Physics Letters* **92** 043510
[7] Rohde C, Choi B J, Jeong D S, Choi S, Zhao J S and Hwang C S 2005 *Applied Physics Letters* **86** 262907
[8] Wang W, Fujita S and Wong S S 2009 *IEEE Electron Device Letters* **30** 763 ISSN 1558-0563
[9] Yang J J, Miao F, Pickett M D, Ohlberg D A A, Stewart D R, Lau C N and Williams R S 2009 *Nanotechnology* **20** 215201
[10] Yang J J, Pickett M D, Li X, Ohlberg D A A, Stewart D R and Williams R S 2008 *Nature Nanotechnology* **3** 429 ISSN 1748-3395
[11] Lu Y, Gao B, Fu Y, Chen B, Liu L, Liu X and Kang J 2012 *IEEE Electron Device Letters* **33** 306
[12] Gao B, Yu S, Xu N, Liu L F, Sun B, Liu X Y, Han R Q, Kang J F, Yu B and Wang Y Y 2008 *2008 IEEE International Electron Devices Meeting* 1
[13] Baek G H, Lee A R, Kim T Y, Im H S and Hong J P 2016 *Applied Physics Letters* **109** 143502
[14] Hsieh C C, Roy A, Rai A, Chang Y F and Banerjee S K 2015 *Applied Physics Letters* **106** 173108
[15] Padovani A, Larcher L, Pirrotta O, Vandelli L and Bersuker G 2015 *IEEE Transactions on Electron Devices* **62** 1998 ISSN 1557-9646
[16] Jalili K, Aghabeygi S and Mirza B 2016 *Journal of Applied Chemical Research* **10** 123
[17] Plotnikov E N and Stolyarova V L 2005 *Physics and Chemistry of Glasses* **46** 187 ISSN 0031-9090
[18] Wen Wu, Xiaodong Duan and Yuan J S 2003 *IEEE Transactions on Device and Materials Reliability* **3** 26
[19] Srivastava S, Dey P, Asapu S and Maiti T 2018 *Nanotechnology* **29** 505702
[20] Mardare D, Baban C, Gavrila R, Modreanu M and Rusu G 2002 *Surface Science* **507-510** 468 ISSN 0039-6028
[21] Bousoulas P, Giannopoulos I, Asenov P, Karageorgiou I and Tsoukalas D 2017 *Journal of Applied Physics* **121** 094501
[22] Yu S and Wong H P 2010 *IEEE Electron Device Letters* **31** 1455

Declaration of interests

☒ The authors declare that they have no known competing financial interests or personal relationships that could have appeared to influence the work reported in this paper.

☐The authors declare the following financial interests/personal relationships which may be considered as potential competing interests:

CRediT author statement

Kuan Yang: Conceptualization, Methodology, Software, Investigation, Writing – Original draft preparation.
Liping Fu: Investigation, Data Curation, Writing- Original draft preparation.
Junhao Chen: Conceptualization, Formal Analysis, Writing- Reviewing and Editing.
Fangcong Wang: Supervision.
Lixue Tian: Resources.
Xiaoqiang Song: Resources.
Zewei Wu: Resources.
Yingtao Li: Conceptualization, Investigation, Data Curation, Supervision, Writing- Reviewing and Editing, Funding acquisition.